Applied Physics Letters

RESEARCH ARTICLE | AUGUST 14 2023

Measuring the anisotropic permittivity tensor of $DyScO_3$ to 110 GHz

Florian Bergmann ; Meagan C. Papac ; Nicholas R. Jungwirth ; Bryan T. Bosworth; Tomasz Karpisz ; Lucas Enright ; Anna Osella ; Eric J. Marksz ; Angela C. Stelson ; Christian J. Long ; Nathan D. Orloff

Appl. Phys. Lett. 123, 072902 (2023)
https://doi.org/10.1063/5.0160460

Applied Physics Letters ARTICLE pubs.aip.org/aip/apl

Measuring the anisotropic permittivity tensor of $DyScO_3$ to 110 GHz

Cite as: Appl. Phys. Lett. **123**, 072902 (2023); doi: 10.1063/5.0160460
Submitted: 1 June 2023 · Accepted: 2 August 2023 ·
Published Online: 14 August 2023

Florian Bergmann,[1,2] Meagan C. Papac,[1] Nicholas R. Jungwirth,[1] Bryan T. Bosworth,[1] Tomasz Karpisz,[1,2] Lucas Enright,[1,3] Anna Osella,[1,3] Eric J. Marksz,[1] Angela C. Stelson,[1] Christian J. Long,[1] and Nathan D. Orloff[1,a)]

AFFILIATIONS

[1]Communications Technology Laboratory, National Institute of Standards and Technology, 325 Broadway, Boulder, Colorado 80305, USA
[2]Department of Physics, University of Colorado, Libby Dr, Boulder, Colorado 80302, USA
[3]Metallurgical and Materials Engineering Department, Colorado School of Mines, 1500 Illinois St., Golden, Colorado 80401, USA

[a)]Author to whom correspondence should be addressed: orloff@nist.gov

ABSTRACT

$DyScO_3$ (DSO) is an attractive substrate on which to grow epitaxial thin films with extraordinary materials physics. However, its highly anisotropic permittivity makes some measurements exceedingly difficult: For instance, its permittivity tensor has not yet been fully characterized at millimeter-wave frequencies. While there are methods to characterize anisotropic permittivity at millimeter-wave frequencies, there are very few methods those are suitable for the small lateral dimensions that $DyScO_3$ can be grown in. To overcome this lack in the material characterization, we tested an on-wafer method based on coplanar waveguides to measure the full anisotropic permittivity tensor from 0.1 to 110 GHz. We characterized two orthogonal sets of coplanar waveguides fabricated on each of two substrates with (001) and (110) crystallographic orientations to resolve the full permittivity tensor. To validate our measurements, we compared our results to data from dc parallel plate capacitors and THz time-domain spectroscopy. Our measurements fill the need for measurements of the permittivity of $DyScO_3$, while the methodology, more generally, enables quantitative characterization of anisotropic dielectrics.

Published by AIP Publishing. https://doi.org/10.1063/5.0160460

$DyScO_3$ (DSO) is a common perovskite substrate used to grow epitaxial thin films. Many materials systems grown on DSO show extraordinary materials physics.[1–8] For instance, recent dielectric–ferroelectric superlattices grown on DSO exhibit polar vortices, skyrmions, and other extraordinary materials states.[9–11] These materials states are possible because DSO induces a biaxial in-plane strain on epitaxially grown perovskite films due to a lattice mismatch on the order of 1%.[1,12] However, DSO has an anisotropic permittivity[13,14] that restricts the available methods to characterize its dielectric properties in the millimeter-wave frequency range. Yet, it is the high frequency range that is of high interest for perovskite epitaxial films.[7,15]

In the low GHz range ($\sim$0.3 to 30 GHz), anisotropic dielectrics have been characterized as inserts in rectangular waveguides,[16] with dual-mode strip line[17] resonators and cavity resonators.[18] In the millimeter-wave range ($\sim$30 to 300 GHz, "mmWaves"), there are only a handful of techniques those can access the complete complex permittivity tensor for anisotropic dielectrics. For example, between 10 and 110 GHz, metrologists can use balanced circular disk resonators to measure out-of-plane permittivity[19] and Fabry–Pérot open resonators for in-plane permittivity[20] of disk-shaped samples. However, both techniques require sample sizes those are larger than the commonly available geometry ($10 \times 10\,mm^2$) of substrates those are difficult to grow, including DSO. For DSO, the literature contains data from parallel plate capacitor measurements of the permittivity at 10 kHz,[14] microwave resonator measurements at 10 GHz,[21] and in-plane time-domain transmission experiments at 200 GHz[22] and above.[23] Nevertheless, both microwave resonator and time-domain transmission measurements do not access the full permittivity tensor. These frequency gaps in the literature provide an opportunity to develop a broadband measurement method for anisotropic permittivity at mmWave frequencies.

Even though there are relatively few methods to measure the anisotropic permittivity tensor, there are many techniques to measure permittivity of isotropic dielectrics. Most broadband methods for measuring the permittivity of isotropic materials use on-wafer devices, such as interdigitated capacitors and transmission lines, such as coplanar waveguides (CPWs).[24] CPWs enable broadband measurements because they support a single, quasi-transverse electromagnetic (TEM) mode. Our hypothesis is that we can engineer CPWs to interact with different elements of the permittivity tensor and then resolve the individual components with multiple CPW orientations relative to the crystal.

In the following, we report an experiment in which we measured two sets of CPWs oriented orthogonal to each other on (001)- and (110)-oriented DSO substrates to measure the full anisotropic permittivity tensor of DSO up to 110 GHz. We discuss the design and fabrication of the CPWs, the scattering (S-) parameter measurements, finite-element field simulations, and the data analysis to extract the complex permittivity. We compare our full anisotropic permittivity tensor to values reported at both lower and higher frequencies. Finally, we address how our measurements could be extended to thin films and what considerations must be made for highly anisotropic materials.

CPWs are a type of planar transmission line. They consist of a center conductor electrode separated from two ground plane electrodes by a gap [Figs. 1(a) and 1(b)]. Transmission lines are typically represented as distributed circuits that consist of a distributed resistance R, inductance L, capacitance C, and conductance G[25] [Fig. 1(c)]. These circuit parameters describe how current and voltage propagate along the transmission line. Applying Kirchhoff's laws, we can derive a characteristic impedance Z and a propagation constant γ that describe the distributed attenuation and phase shift,

$$\gamma = \sqrt{R + i\omega L} \times \sqrt{G + i\omega C}, \tag{1}$$

$$Z = \sqrt{R + i\omega L} / \sqrt{G + i\omega C}. \tag{2}$$

For better readability, Eqs. (1) and (2) omit the explicit frequency dependence of each circuit parameter. CPWs support a quasi-TEM-mode [Fig. 1(d)]. In this quasi-TEM approximation, R and L depend on the shape of the electrodes, the conductor properties of the electrodes, and the magnetic properties of the substrate. On the other hand, C and G depend on the shape of the electrodes and the dielectric properties of the substrate. Furthermore, in the quasi-TEM approximation, C is only sensitive to permittivity tensor elements those are perpendicular to the Poynting vector. Strictly speaking, anisotropy has the potential to invalidate the quasi-TEM approximation. We will address this issue below. Our hypothesis is that orienting the CPW along at least three different crystallographic directions can perturb the distributed circuit parameters of the CPWs in such a way that we gain access to the full permittivity tensor. The permittivity tensor is diagonal in the principal coordinate system of the crystal, ε_{dia}, and is symmetric in the measurement coordinate system of the CPW, ε_{CPW}:

$$\varepsilon_{dia} = \begin{pmatrix} \varepsilon_a & 0 & 0 \\ 0 & \varepsilon_b & 0 \\ 0 & 0 & \varepsilon_c \end{pmatrix} \quad \text{and} \quad \varepsilon_{CPW} = \begin{pmatrix} \varepsilon_{xx} & \varepsilon_{xy} & \varepsilon_{xz} \\ \varepsilon_{xy} & \varepsilon_{yy} & \varepsilon_{yz} \\ \varepsilon_{xz} & \varepsilon_{yz} & \varepsilon_{zz} \end{pmatrix}, \tag{3}$$

where ε_a, ε_b, and ε_c are parallel to DSO's respective lattice vectors with lengths a = 5.4 Å, b = 5.7 Å, and c = 7.9 Å.[13] We chose the orthorhombic notation rather than the pseudo-cubic notation that is also present in the literature.[9,26]

We fabricated CPW transmission lines on (001)- and (110)-oriented 10 × 10 mm^2 DSO chips with conventional lithographic techniques and electron-beam deposition. The electrodes were nominally 500 nm thick gold with a 10 nm titanium adhesion layer. Our chip layout included a short-circuit reflect and a set of CPW transmission lines with lengths ℓ = 0.420, 0.720, 1.040, 2.30, 3.060, and 4.000 mm. These devices are the necessary standards to perform the multiline thru-reflect-line (mTRL) algorithm.[27] We arranged the CPWs such that the Poynting vectors were oriented along the [100], [010], [001], and [1$\bar{1}$0] crystal planes (Fig. 2). The alignment of the substrate is delivered by the manufacturer with a 0.5° tolerance, and the alignment uncertainty

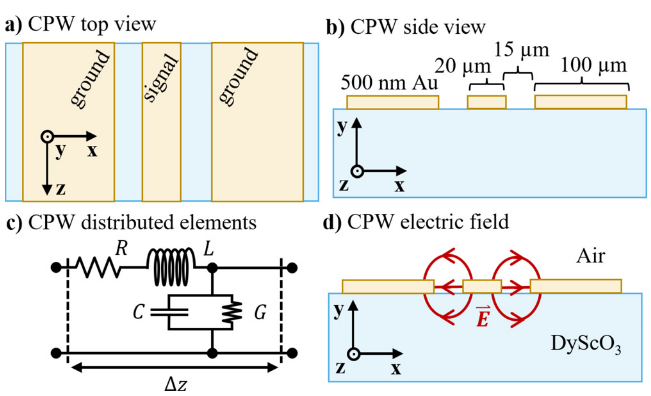

FIG. 1. Schematic of a CPW. (a) top view, (b) side view with dimensions, (c) representation of the CPW as transmission line with distributed resistance R, inductance L, capacitance C, and conductance G, and (d) side view with sketched electric field pattern of the quasi-TEM CPW mode.

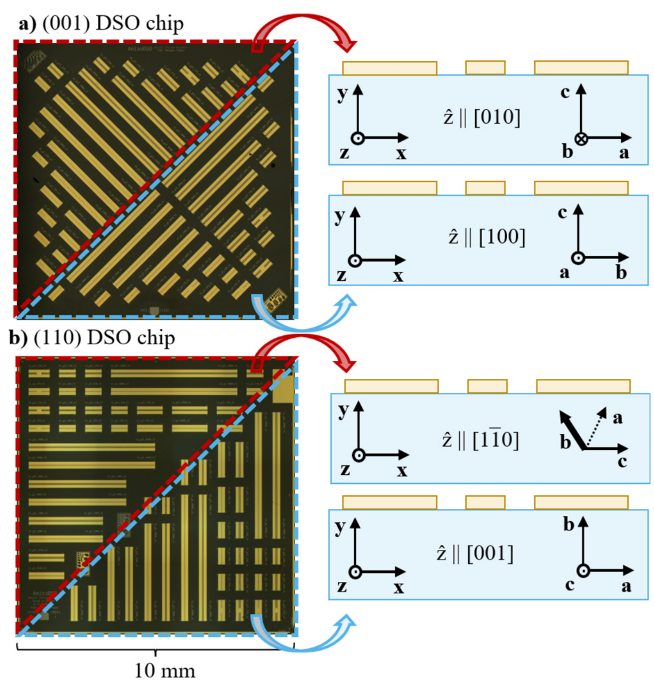

FIG. 2. Top view optical microscope image of the (a) (001)-oriented and the (b) (110)-oriented $DyScO_3$ chip. Each image has a schematic of CPWs attached, comparing the relative orientation of the crystal's coordinate system (a-b-c) and the CPW's coordinate system (x-y-z).

of our lithography is within 1°. By evaluating changes in the permittivity tensor under small rotations, we estimate the impact of a misalignment within that tolerance on the extracted permittivity ε_r to give an error less than $\Delta\varepsilon_r < 0.05$.

We checked the lateral dimensions of the center conductor, gaps, and ground plane widths with an optical microscope, which we calibrated using a known-length standard. This measurement confirmed the nominal lateral geometry within a standard uncertainty of 1 μm. We determined the conductor thicknesses with stylus profilometry. Our conductors were (470 ± 10) nm thick. We measured a single pair of dc currents and voltages with a source-measure unit to extract the center conductor dc resistance of each CPW. We fit the resistance of all the lines vs length to extract the distributed dc resistance.

We contacted each CPW device with ground-signal-ground probes and measured S-parameters with a vector network analyzer. Our experimental design used a two-tier calibration approach.[28] The first-tier used CPW standards patterned on a (001)-oriented $(LaAlO_3)_{0.3}(Sr_2TaAlO_6)_{0.7}$ (LSAT)[29] substrate with nominally identical cross section geometries to the devices on the DSO chips. Additionally, the larger 2-in. LSAT wafer allowed us to include longer lines ($\ell = 5.660$, 7.180, and 9.580 mm). We chose LSAT ($\varepsilon_r \approx 23$) because it has a permittivity that is comparable to DSO, which improved the accuracy of the first-tier calibration by reducing systematic errors due to the probe contact.[28] For the first-tier calibration, we used the mTRL algorithm[27] and a series resistor calibration[30,31] to set the reference impedance. This first tier corrects the S-parameters of the devices on DSO to 50 Ω at the reference planes of the probe tips. The second-tier calibration consists of a second application of the mTRL algorithm on the corrected S-parameters of the devices for each CPW orientation. These second-tier calibrations produced a separate γ_{TRL} and Z_{TRL} for the [100], [010], [001], and [1$\bar{1}$0] orientations.[32–34]

We compared two different techniques for extracting the distributed circuit parameters. The first technique assumed that the substrate was nondispersive, which allowed us to set $G(\omega) = 0$ and $C(\omega) = C_0$. This technique lost information about the material's dielectric loss but provided a low-noise R and L that can be precisely compared against those from finite-element simulations. We computed C as

$$C = \mathrm{Im}(\gamma_{TRL}/Z_{TRL})/\omega. \tag{4}$$

Next, we averaged C in the optimal decade for impedance extraction from 1 GHz to 10 GHz to get C_o and used the standard deviation of C as the uncertainty. We use this C_o to get $R_{G=0}$ and $L_{G=0}$ from γ_{TRL},

$$R_{G=0} + \mathrm{i}\omega L_{G=0} = \gamma_{TRL}^2/(i\omega C_0). \tag{5}$$

We compared $R_{G=0}$ and $L_{G=0}$ to those from finite-element field simulations, R_{sim} and L_{sim}. In these simulations, we implemented the measured conductor thickness from stylus profilometry. Next, we assumed that our lithography process gives the nominal lateral geometry plus or minus a length δ due to a consistent over- or underdevelopment of the photoresist over the whole chip. This assumption leaves a single fit parameter (the length δ) to adjust L_{sim} to $L_{G=0}$. We obtained values in the range $\delta = \pm 0.3\,\mu$m. By varying δ, we also computed the uncertainty ΔL_{sim} from values that still agree with the measured $L_{G=0}$ within the uncertainty $\Delta L_{G=0}$. Through this fit, we extracted the actual electromagnetically relevant lateral dimensions of the electrodes. These δ-corrected dimensions agree with the values from the optical microscopy but offer a higher precision by one order of magnitude (0.1 vs 1 μm). From dc resistance and the δ-corrected conductor dimensions, we calculated a resistivity of $(2.8 \pm 0.1)\,\mu\Omega\,$cm, which is comparable to other reports of electron-beam-deposited gold.[35] We used the δ-corrected dimensions to extract the permittivity ε_r from the distributed capacitance C. Because this technique made several assumptions, we compared it to an independent second technique. The second technique directly fits the distributed circuit elements R, L, C, and G to the corrected S-parameters using a mismatched transmission line model.[36] The latter technique made the fewest assumptions about the material but resulted in larger uncertainties.

To complete our analysis, we performed finite-element field simulations to map the distributed capacitance C to the permittivity ε_r. The C of a CPW depends on the in-plane ε_{xx}, the out-of plane ε_{yy}, and the off diagonal ε_{xy}, $C = C(\varepsilon_{xx}, \varepsilon_{yy}, \varepsilon_{xy})$. In our mapping simulations, we varied each relevant element of the permittivity tensor (ε_{xx}, ε_{yy}, and ε_{xy}) independently and computed C for that combination of values. We implemented a set of CPWs in 3D simulations for a mTRL calibration and extracted the propagation constant γ_{3D}. We then used the distributed inductance L_{2D} and resistance R_{2D} from 2D simulations of the CPW's cross section to get the distributed capacitance C,

$$C = \mathrm{Im}\left(\frac{\gamma_{3D}^2}{R_{2D} + i\omega L_{2D}}\right)\Big/\omega. \tag{6}$$

In the mapping function $C(\varepsilon_{xx}, \varepsilon_{yy}, \varepsilon_{xy})$, the convolution of ε_{xx}, ε_{yy}, and ε_{xy} is generally nonlinear. Here, we present locally linear sections of the function that we obtained from our simulations,

$$\begin{aligned}
C_{[100]}[\mathrm{pF/cm}] &= (11.0 \pm 0.3)\times 10^{-2} + (7.86 \pm 0.01)\times 10^{-2}\varepsilon_b \\
&\quad + (4.67 \pm 0.04)\times 10^{-2}\varepsilon_c \\
C_{[010]}[\mathrm{pF/cm}] &= (10.6 \pm 0.8)\times 10^{-2} + (7.81 \pm 0.04)\times 10^{-2}\varepsilon_a \\
&\quad + (4.65 \pm 0.01)\times 10^{-2}\varepsilon_c, \\
C_{[001]}[\mathrm{pF/cm}] &= (12.8 \pm 0.3)\times 10^{-2} + (4.22 \pm 0.02)\times 10^{-2}\varepsilon_a \\
&\quad + (8.16 \pm 0.05)\times 10^{-2}\varepsilon_b
\end{aligned}$$

and

$$\begin{aligned}
C_{[1\bar{1}0]}[\mathrm{pF/cm}] &= (12 \pm 3)\times 10^{-2} + (3.93 \pm 0.01)\times 10^{-2}(\varepsilon_a + \varepsilon_b) \\
&\quad + (4.77 \pm 0.05)\times 10^{-2}\varepsilon_c.
\end{aligned}$$

The first term in all these equations relate to the contribution of air to C. They differ because of the differences in the δ-corrected conductor geometry in each orientation. The equations $C_{[100]}$, $C_{[010]}$, and $C_{[001]}$ describe a set of planes with large angles between pairs of them: $\measuredangle(C_{[100]}, C_{[010]}) = 75°$, $\measuredangle(C_{[100]}, C_{[001]}) = 40°$, and $\measuredangle(C_{[010]}, C_{[001]}) = 67°$. This geometry offers precise determination of the permittivity. Together with $C_{[1\bar{1}0]}$, we obtain a set of four equations that contain three unknowns $\varepsilon_a, \varepsilon_b$, and ε_c. We used the relation $\tan\delta = \varepsilon''/\varepsilon' = G/\omega C$ to extract the dielectric loss tangent. We also simulated an isotropic substrate of comparable permittivity and verified our 2D and 3D simulations against results from the high and low frequency limit of analytic conformal mapping.[37] We found a maximum deviation of 0.02%, which is more than one order of magnitude below the measurement uncertainly.

We compared our results from the different analysis techniques in terms of the distributed inductance L, distributed resistance R, permittivity ϵ_r, and dielectric loss $\tan\delta$ (Fig. 3). L and R from our different analysis techniques agreed within their respective uncertainties up to 30 GHz [Figs. 3(a) and 3(b)]. The general frequency trend of L and

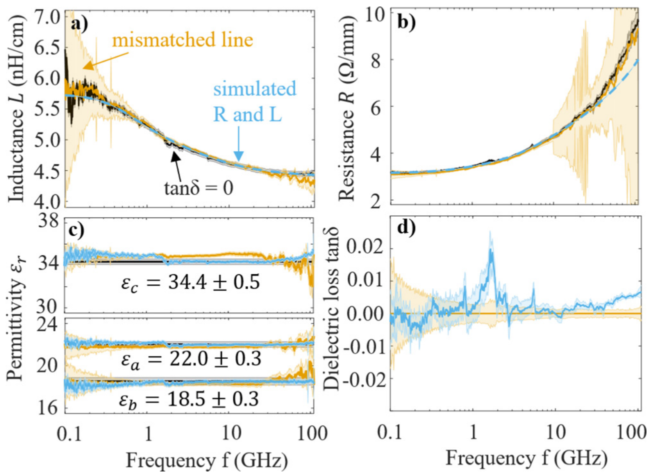

FIG. 3. Extracted circuit parameters. (a) Distributed inductance L, (b) distributed resistance R, (c) permittivity ε_r derived from the distributed capacitance C, and (d) dielectric loss tanδ derived from the distributed conductivity G. All subfigures show the extracted parameters for the nondispersive substrate assumption $R_{G=0}$, $L_{G=0}$, and $C_{G=0}$, for the fitted R_{sim} and L_{sim} from finite element simulations, and for the mismatched transmission line model. Shaded areas are the 1-sigma uncertainty.

R is due to the skin effect.[38] At frequencies above 30 GHz, we found that the simulation underestimated L and R when compared to the measurement values. While the discrepancy in R is clearly visible [Fig. 3(b)], the discrepancy in L is more apparent in the upturn of the permittivity derived from the simulated R_{sim} and L_{sim} [Fig. 3(c)]. We currently do not understand the source of the additional R and deviating L. We are aware that for our geometry, the critical frequency of the dielectric slab mode is around 40 GHz. Nevertheless, we excluded higher order modes and conductor roughness being responsible for the deviations in R and L.[39] We conclude that even if higher order modes are present, they have a negligible effect on our measurements. The uncertainty in L is large at low frequencies because the phase difference accumulated over the CPW length is small, leading to a large relative uncertainty of the phase. It is mainly the phase that influences the extraction of L. On the other hand, the uncertainty of the extracted R using the mismatched line fit is large at high frequencies due the fitting algorithm, which gives rise to large relative uncertainties at low transmission.

We observed a small peak in all elements of the permittivity and an increased dielectric loss at around 1.3 GHz. We also do not understand the source of this peak. However, we encountered it in many on-wafer measurements at a similar frequency, independent of the substrate material.[40] Hence, we do not expect that this peak is due to the specific material properties of DSO, rather it is likely due to a systematic error in the measurement. The agreement between the applied analysis techniques confirmed that the extracted $\tan\delta$ was negligible compared to our measurement uncertainties. We note there are frequencies where the loss tangent is negative. At these frequencies, the loss tangent is below our measurement sensitivity. While longer lines could improve the measurement sensitivity, the $10 \times 10\,\mathrm{mm}^2$ of DSO substrates limited the maximum length of the line we could fabricate.

This result implies that, for most on-wafer applications, DSO can be approximated as a lossless and therefore nondispersive material. For this approximation, we extracted $C_{[100]} = 3.17 \pm 0.02\,\mathrm{pF/cm}$, $C_{[010]} = 3.46 \pm 0.02\,\mathrm{pF/cm}$, $C_{[001]} = 2.71 \pm 0.02\,\mathrm{pF/cm}$, and $C_{[1\bar{1}0]} = 3.32 \pm 0.02\,\mathrm{pF/cm}$. We summarized our results on the permittivity of DSO in Table I and compared them against the literature. The uncertainty in the extracted permittivity is dominated by the uncertainty in determination of the CPW gap width and the random variation of the extracted distributed capacitance over the frequency range 1–10 GHz. The denoted uncertainty in the extracted permittivity does not include any possible systematic errors done in the first-tier calibration. We also applied our techniques to the LSAT wafer that we used as a first-tier calibration. We obtained $\varepsilon_r = 23.4 \pm 0.1$, which is comparable to prior reports of $\varepsilon_r = 23.1 \pm 0.3$ up to 40 GHz[41] and $\varepsilon_r = 22.5$ at 10 GHz.[29]

We acknowledge some additional considerations and limitations of our approach. We initially considered varying the gap width of the CPW to access the anisotropic permittivity. However, our simulations showed that the sensitivity of C to differentiate between in-plane and out-of-plane permittivity in large vs small gap width configurations is small compared to our typical measurement uncertainty in C. This would result in larger than desired uncertainties in the permittivity ϵ_r. Fundamentally, our analysis techniques make two assumptions that may not be true for all systems. First, we assumed that DSO is nonmagnetic, which is reasonable at room temperature but not at very low temperatures.[26] Second, we assumed the mode in the CPW as quasi-TEM. The non-zero ε_{yz} element of the permittivity in the $[1\bar{1}0]$ configuration (Fig. 2) strictly breaks this assumption. However, we estimated the induced displacement current to be about six orders of magnitude below the charge current in the conductor and therefore neglected it. Still, for highly anisotropic substrates or thin films, we expect that it is necessary to take this displacement current into account.

In conclusion, the objective of this work was to test a methodology for measuring the anisotropic permittivity tensor of substrates. To test our methodology, we chose $DyScO_3$ because it is an important substrate for materials discovery and its anisotropic permittivity has not been fully characterized above 10 kHz, but there are values in the literature for its permittivity at discrete frequencies for comparison. We used two orthogonal CPW-based materials characterization kits patterned on (001)- and (110)-oriented $10 \times 10\,\mathrm{mm}^2$ $DyScO_3$ chips. These orthogonal kits allowed us to obtain the anisotropic permittivity tensor by extracting the distributed capacitances in four different crystallographic orientations. For $DyScO_3$, we obtained values and standard uncertainties of $\epsilon_a = 22.0 \pm 0.3$, $\epsilon_b = 18.5 \pm 0.3$, and $\epsilon_c = 34.4 \pm 0.5$ for the three elements of the permittivity tensor from 0.1 to 110 GHz. We also obtained a dielectric loss tangent $\tan\delta$ below 0.01 for each element of the tensor. Our permittivity values are consistent with previously reported findings at 10 kHz and 200 GHz. More

TABLE I. Comparison of the anisotropic permittivity of DSO extracted in different frequency ranges at room temperature.

	10 kHz[14]	100 MHz–110 GHz (this work)	200 GHz[22]
ε_a	21.9	22.0 ± 0.3 ($\tan\delta < 0.01$)	$\varepsilon_{(110)} = 21$
ε_b	18.9	18.5 ± 0.3 ($\tan\delta < 0.01$)	($\tan\delta = 0.005$)
ε_c	33.8	34.4 ± 0.5 ($\tan\delta < 0.01$)	34 ($\tan\delta = 0.02$)

broadly, this methodology highlights an approach for quantitative dielectric characterization of anisotropic substrates. Extensions of this work could be applied to in-plane permittivity characterization of anisotropic thin films, which may be limited to in-plane measurements only depending on film's thickness. At present, there is industry demand to revisit out-of-plane permittivity characterization and extend or redevelop existing methodologies to millimeter-waves.

In summary, before this work there were few methodologies for characterizing the anisotropic permittivity tensor up to 110 GHz and there was no microwave- or millimeter-wave characterization of the complete anisotropic permittivity tensor of $DyScO_3$ reported in the literature. After this work, there is an approach for characterizing anisotropic substrates that may have significant impacts in semiconductor manufacturing of next-generation communications technology.

The authors thank the critical review of S. R. Evans, N. Tomlin, and J. C. Booth, all with the National Institute of Standards and Technology (NIST), for their critical feedback during this research, and their comments on this paper's manuscript. The authors also thank O. Krivosudsky for support on the full wave simulations and A. Hagerstrom for discussions on the theory of anisotropic dielectrics. This paper is an official contribution of NIST, not subject to copyright in the US. Usage of commercial products herein is for information only; it does not imply recommendation or endorsement by NIST.

AUTHOR DECLARATIONS

Conflict of Interest

The authors have no conflicts to disclose.

Author Contributions

Florian Bergmann: Conceptualization (lead); Formal analysis (lead); Methodology (lead); Writing – original draft (equal). **Christian J. Long:** Methodology (supporting); Supervision (supporting). **Nathan Orloff:** Conceptualization (supporting); Funding acquisition (lead); Project administration (lead); Resources (equal); Software (equal); Supervision (lead); Writing – original draft (equal). **Meagan Papac:** Resources (equal); Writing – review & editing (lead). **Nicholas Ryan Jungwirth:** Methodology (supporting). **Bryan T. Bosworth:** Software (equal). **Tomasz Karpisz:** Software (equal). **Lucas Enright:** Methodology (supporting); Writing – review & editing (supporting). **Anna Osella:** Methodology (supporting). **Eric Marksz:** Conceptualization (supporting); Methodology (supporting). **Angela Stelson:** Software (equal).

DATA AVAILABILITY

The data that support the findings of this study are available from the corresponding author upon reasonable request.

REFERENCES

[1] J. H. Haeni, P. Irvin, W. Chang, R. Uecker, P. Reiche, Y. L. Li, S. Choudhury, W. Tian, M. E. Hawley, B. Craigo, A. K. Tagantsev, X. Q. Pan, S. K. Streiffer, L. Q. Chen, S. W. Kirchoefer, J. Levy, and D. G. Schlom, "Room-temperature ferroelectricity in strained $SrTiO_3$," Nature **430**, 758 (2004).

[2] K. J. Choi, M. Biegalski, Y. L. Li, A. Sharan, J. Schubert, R. Uecker, P. Reiche, Y. B. Chen, X. Q. Pan, V. Gopalan, L.-Q. Chen, D. G. Schlom, and C. B. Eom, "Enhancement of ferroelectricity in strained $BaTiO_3$ thin films," Science **306**(5698), 1005–1009 (2004).

[3] D. G. Schlom, L.-Q. Chen, C.-B. Eom, K. M. Rabe, S. K. Streiffer, and J.-M. Triscone, "Strain tuning of ferroelectric thin films," Annu. Rev. Mater. Res. **37**(1), 589–626 (2007).

[4] A. Vailionis, W. Siemons, and G. Koster, "Room temperature epitaxial stabilization of a tetragonal phase in $ARuO_3$ (A=Ca and Sr) thin films," Appl. Phys. Lett. **93**(5), 051909 (2008).

[5] D. Nuzhnyy, J. Petzelt, S. Kamba, P. Kužel, C. Kadlec, V. Bovtun, M. Kempa, J. Schubert, C. M. Brooks, and D. G. Schlom, "Soft mode behavior in $SrTiO_3$/$DyScO_3$ thin films: Evidence of ferroelectric and antiferrodistortive phase transitions," Appl. Phys. Lett. **95**(23), 232902 (2009).

[6] J. H. Lee, L. Fang, E. Vlahos, X. Ke, Y. W. Jung, L. F. Kourkoutis, J.-W. Kim, P. J. Ryan, T. Heeg, M. Roeckerath, V. Goian, M. Bernhagen, R. Uecker, P. C. Hammel, K. M. Rabe, S. Kamba, J. Schubert, J. W. Freeland, D. A. Muller, C. J. Fennie, P. Schiffer, V. Gopalan, E. Johnston-Halperin, and D. G. Schlom, "A strong ferroelectric ferromagnet created by means of spin–lattice coupling," Nature **466**(7309), 954–958 (2010).

[7] C.-H. Lee, N. D. Orloff, T. Birol, Y. Zhu, V. Goian, E. Rocas, R. Haislmaier, E. Vlahos, J. A. Mundy, L. F. Kourkoutis, Y. Nie, M. D. Biegalski, J. Zhang, M. Bernhagen, N. A. Benedek, Y. Kim, J. D. Brock, R. Uecker, X. X. Xi, V. Gopalan, D. Nuzhnyy, S. Kamba, D. A. Muller, I. Takeuchi, J. C. Booth, C. J. Fennie, and D. G. Schlom, "Exploiting dimensionality and defect mitigation to create tunable microwave dielectrics," Nature **502**(7472), 532–536 (2013).

[8] N. M. Dawley, E. J. Marksz, A. M. Hagerstrom, G. H. Olsen, M. E. Holtz, V. Goian, C. Kadlec, J. Zhang, X. Lu, J. A. Drisko, R. Uecker, S. Ganschow, C. J. Long, J. C. Booth, S. Kamba, C. J. Fennie, D. A. Muller, N. D. Orloff, and D. G. Schlom, "Targeted chemical pressure yields tuneable millimetre-wave dielectric," Nat. Mater. **19**(2), 176–181 (2020).

[9] A. K. Yadav, C. T. Nelson, S. L. Hsu, Z. Hong, J. D. Clarkson, C. M. Schlepütz, A. R. Damodaran, P. Shafer, E. Arenholz, L. R. Dedon, D. Chen, A. Vishwanath, A. M. Minor, L. Q. Chen, J. F. Scott, L. W. Martin, and R. Ramesh, "Observation of polar vortices in oxide superlattices," Nature **530**(7589), 198–201 (2016).

[10] Z. Hong, A. R. Damodaran, F. Xue, S.-L. Hsu, J. Britson, A. K. Yadav, C. T. Nelson, J.-J. Wang, J. F. Scott, L. W. Martin, R. Ramesh, and L.-Q. Chen, "Stability of polar vortex lattice in ferroelectric superlattices," Nano Lett. **17**(4), 2246–2252 (2017).

[11] S. Das, Y. L. Tang, Z. Hong, M. A. P. Gonçalves, M. R. McCarter, C. Klewe, K. X. Nguyen, F. Gómez-Ortiz, P. Shafer, E. Arenholz, V. A. Stoica, S.-L. Hsu, B. Wang, C. Ophus, J. F. Liu, C. T. Nelson, S. Saremi, B. Prasad, A. B. Mei, D. G. Schlom, J. Íñiguez, P. García-Fernández, D. A. Muller, L. Q. Chen, J. Junquera, L. W. Martin, and R. Ramesh, "Observation of room-temperature polar skyrmions," Nature **568**(7752), 368–372 (2019).

[12] Q. Li, V. A. Stoica, M. Paściak, Y. Zhu, Y. Yuan, T. Yang, M. R. McCarter, S. Das, A. K. Yadav, S. Park, C. Dai, H. J. Lee, Y. Ahn, S. D. Marks, S. Yu, C. Kadlec, T. Sato, M. C. Hoffmann, M. Chollet, M. E. Kozina, S. Nelson, D. Zhu, D. A. Walko, A. M. Lindenberg, P. G. Evans, L.-Q. Chen, R. Ramesh, L. W. Martin, V. Gopalan, J. W. Freeland, J. Hlinka, and H. Wen, "Subterahertz collective dynamics of polar vortices," Nature **592**(7854), 376–380 (2021).

[13] B. Veličkov, V. Kahlenberg, R. Bertram, and M. Bernhagen, "Crystal chemistry of $GdScO_3$, $DyScO_3$, $SmScO_3$ and $NdScO_3$," Z. Kristallogr. **222**(9), 466–473 (2007).

[14] S. Coh, T. Heeg, J. H. Haeni, M. D. Biegalski, J. Lettieri, L. F. Edge, K. E. O'Brien, M. Bernhagen, P. Reiche, R. Uecker, S. Trolier-McKinstry, D. G. Schlom, and D. Vanderbilt, "Si-compatible candidates for high-κ dielectrics with the *Pbnm* perovskite structure," Phys. Rev. B **82**(6), 064101 (2010).

[15] S. Das, Z. Hong, V. A. Stoica, M. A. P. Gonçalves, Y. T. Shao, E. Parsonnet, E. J. Marksz, S. Saremi, M. R. McCarter, A. Reynoso, C. J. Long, A. M. Hagerstrom, D. Meyers, V. Ravi, B. Prasad, H. Zhou, Z. Zhang, H. Wen, F. Gómez-Ortiz, P. García-Fernández, J. Bokor, J. Íñiguez, J. W. Freeland, N. D. Orloff, J. Junquera, L. Q. Chen, S. Salahuddin, D. A. Muller, L. W. Martin, and R. Ramesh, "Local

negative permittivity and topological phase transition in polar skyrmions," Nat. Mater. **20**(2), 194–201 (2021).
[16]B. R. Crowgey, O. Tuncer, J. Tang, E. J. Rothwell, B. Shanker, L. C. Kempel, and M. J. Havrilla, "Characterization of biaxial anisotropic material using a reduced aperture waveguide," IEEE Trans. Instrum. Meas. **62**(10), 2739–2750 (2013).
[17]J. C. Rautio, R. L. Carlson, B. J. Rautio, and S. Arvas, "Shielded dual-mode microstrip resonator measurement of uniaxial anisotropy," IEEE Trans. Microwave Theory Techn. **59**(3), 748–754 (2011).
[18]P. Kopyt, B. Salski, and J. Krupka, "Measurements of the complex anisotropic permittivity of laminates with TM_0n_0 cavity," IEEE Trans. Microwave Theory Techn. **70**(1), 432–443 (2022).
[19]Y. Kato and M. Horibe, "Broadband permittivity measurements up to 170-GHz using balanced-type circular-disk resonator excited by 0.8-mm coaxial line," IEEE Trans. Instrum. Meas. **68**(6), 1796–1805 (2019).
[20]B. Salski, T. Karpisz, M. Warecka, P. Kowalczyk, P. Czekala, and P. Kopyt, "Microwave characterization of dielectric sheets in a plano-concave Fabry-Perot open resonator," IEEE Trans. Microwave Theory Techn. **70**(5), 2732–2742 (2022).
[21]V. Bovtun, V. Pashkov, M. Kempa, V. Molchanov, S. Kamba, Y. Poplavko, and Y. Yakymenko, "Anisotropic dielectric substrate as thin dielectric resonator," in *22nd International Crimean Conference "Microwave & Telecommunication Technology,"* Sevastopol, Ukraine (IEEE, 2012), pp. 573–574.
[22]V. Bovtun, V. Pashkov, D. Nuzhnyy, M. Kempa, V. Goian, V. Molchanov, Y. Poplavko, Y. Yakymenko, and S. Kamba, "Microwave and terahertz dielectric properties of single-crystalline scandate substrates for ferroic thin film deposition," in *23rd International Crimean Conference "Microwave & Telecommunication Technology,"* Sevastopol, Ukraine (IEEE, 2013), pp. 646–648.
[23]G. A. Komandin, E. S. Zhukova, V. I. Torgashev, A. V. Boris, A. A. Boris, E. A. Motovilova, A. S. Prokhorov, L. S. Kadyrov, B. P. Gorshunov, and M. Dressel, "Terahertz-infrared spectra of the rare-earth scandate $DyScO_3$ single crystal," J. Appl. Phys. **114**(2), 024102 (2013).
[24]C. P. Wen, "Coplanar waveguide: A surface strip transmission line suitable for nonreciprocal gyromagnetic device applications," IEEE Trans. Microwave Theory Techn. **17**(12), 1087–1090 (1969).
[25]R. B. Marks and D. F. Williams, "A general waveguide circuit theory," J. Res. Natl. Inst. Stan. **97**(5), 533 (1992).
[26]X. Ke, C. Adamo, D. G. Schlom, M. Bernhagen, R. Uecker, and P. Schiffer, "Low temperature magnetism in the perovskite substrate $DyScO_3$," Appl. Phys. Lett. **94**(15), 152503 (2009).
[27]R. B. Marks, "A multiline method of network analyzer calibration," IEEE Trans. Microwave Theory Techn. **39**(7), 1205–1215 (1991).
[28]D. F. Williams, U. Arz, and H. Grabinski, in *1998 IEEE MTT-S International Microwave Symposium Digest (Cat. No.98CH36192)* (IEEE, Baltimore, MD, 1998), pp. 1917–1920.
[29]S. C. Tidrow, A. Tauber, W. D. Wilber, R. T. Lareau, C. D. Brandle, G. W. Berkstresser, A. J. Ven Graitis, D. M. Potrepka, J. I. Budnick, and J. Z. Wu, "New substrates for HTSC microwave devices," IEEE Trans. Appl. Supercond. **7**(2), 1766–1768 (1997).
[30]D. F. Williams and D. K. Walker, in *50th ARFTG Conference Digest* (IEEE, Portland, OR, 1997), pp. 131–137.
[31]J. A. Drisko, R. A. Chamberlin, J. C. Booth, N. D. Orloff, and C. J. Long, "Optimal series resistors for on-wafer calibrations," IEEE Trans. Microwave Theory Techn. **68**(1), 196–210 (2020).
[32]D. F. Williams, R. B. Marks, and A. Davidson, in *38th ARFTG Conference Digest* (IEEE, San Diego, CA, 1991), pp. 68–81.
[33]M. D. Janezic and J. A. Jargon, "Complex permittivity determination from propagation constant measurements," IEEE Microwave Guid. Wave Lett. **9**(2), 76–78 (1999).
[34]R. B. Marks and D. F. Williams, "Characteristic impedance determination using propagation constant measurement," IEEE Microwave Guid. Wave Lett. **1**(6), 141–143 (1991).
[35]J. R. Sambles, K. C. Elsom, and D. J. Jarvis, "The electrical resistivity of gold films," Philos. Trans. R. Soc., A **304**(1486), 365–396 (1982).
[36]N. D. Orloff, N. Popovic, J. A. Drisko, A. Stelson, C. A. E. Little, J. C. Booth, J. Mateu, and C. J. Long, in *2017 90th ARFTG Microwave Measurement Symposium (ARFTG)* (IEEE, Boulder, CO, 2017), pp. 1–5.
[37]W. Heinrich, "Quasi-TEM description of MMIC coplanar lines including conductor-loss effects," IEEE Trans. Microwave Theory Techn. **41**(1), 45–52 (1993).
[38]H. A. Wheeler, "Formulas for the skin effect," Proc. IRE **30**(9), 412–424 (1942).
[39]F. Bergmann, N. Jungwirth, B. Bosworth, J. Killgore, E. Marksz, T. Karpisz, M. Papac, A. Osella, L. Enright, C. J. Long, and N. D. Orloff, "Testing dielectric slab mode excitation, non-rectangular conductor profiles and edge roughness as sources of additional loss in mmWave transmission lines," in 2023 IEEE/MTT-S International Microwave Symposium – IMS 2023, San Diego, CA, USA, 2023 (IEEE, 2023), pp. 366–369.
[40]N. D. Orloff, J. Mateu, A. Lewandowski, E. Rocas, J. King, D. Gu, X. Lu, C. Collado, I. Takeuchi, and J. C. Booth, "A compact variable-temperature broadband series-resistor calibration," IEEE Trans. Microwave Theory Techn. **59**(1), 188–195 (2011).
[41]N. D. Orloff, W. Tian, C. J. Fennie, C. H. Lee, D. Gu, J. Mateu, X. X. Xi, K. M. Rabe, D. G. Schlom, I. Takeuchi, and J. C. Booth, "Broadband dielectric spectroscopy of Ruddlesden–Popper $Sr_{n+1}TiO_{3n+1}$ (n=1,2,3) thin films," Appl. Phys. Lett. **94**(4), 042908 (2009).